Optimisation of analyte transport in integrated microfluidic affinity sensors for the quantification of low levels of analyte

Optimisation of analyte transport in integrated microfluidic affinity sensors for the quantification of low levels of analyte

Daniel Friedrich [a], Colin Please [b], Tracy Melvin [a,*]

[a] *Optoelectronics Research Centre, University of Southampton, Highfield, SO17 1BJ, UK*

[b] *School of Mathematics, University of Southampton, Highfield, SO17 1BJ, UK*

Preprint submitted to Elsevier *21 November 2013*

Abstract

New designs for microfluidic channels to be integrated with small scale affinity sensors for analytical applications are provided. Theoretical approaches demonstrate efficient and uniform mass- transfer of the analyte from the bulk flow to small scale affinity sensors in the base of fluidic channels by (i) active control of the analyte flow speed over the affinity sensor, (ii) non-rectangular channel geometries and (iii) non-uniform distributions of recognition binding sites over the active area of the sensor. The methodology reported provides generic strategies that can be exploited for small scale sensors in single or multiplex formats.

Key words: affinity sensor, microfluidics, mass transfer, laminar flow, biosensor, fluidic channel, detection, design optimisation, recognition molecule, analyte depletion

* Corresponding author. Tel: +44(0)2380596505, Fax: +44(0)2380593149, Email: tm@orc.soton.ac.uk

[A]	analyte concentration
$[A_0]$	input analyte concentration
α	binding/convection number
[B]	bound analyte concentration
D	diffusion coefficient
Da	Damköhler number
$g(x)$	active/inactive area boundary
Gz	Graetz number
$H(x)$	Heaviside function
H	channel height
k_a	forward rate constant
κ	adsorption capacity
L	channel length
n_g	inner normal of the active/inactive interface
p, p_1, p_2	pressure fields
S	active area
t	time variable
$u(t)$	variable flow velocity

U	mean flow velocity
$W(x)$	channel width
[X]	receptor concentration
$[X_0]$	initial receptor concentration
$[X_s](x)$	variable receptor concentration
x, y, z	spatial variables

1 Introduction

Integrated affinity sensors, within microfluidic structures, are receiving much attention for life science and environmental analytical science applications [1, 2]. These affinity sensors are typically positioned in the base of a fluidic flow channel over which an analyte solution is passed. The detection of the analyte on the sensor is dependent upon a recognition-binding event, most typically antibody-antigen or DNA hybridisation, where the recognition molecules for the analyte are attached to the surface of the sensor. The recognition molecule-analyte complex is detected on the sensor, for example by optical means (i.e. fluorescence [3] or surface plasmon resonance [4]). These integrated affinity sensors have two key applications i) the evaluation of binding parameters for biomolecular recognition between one immobilised molecule and another in solution (as developed by companies such as Biacore), and ii) the quantification of low levels of analyte by association with a recognition molecule that is immobilised on the sensor. The fluidic structures and the operation requirements

used for these affinity sensor systems are quite different. The fluidic structures integrated with affinity sensors for the evaluation of the binding parameters for biomolecular recognition have been well considered [5, 6]. Here the rate of change of the affinity sensor signal must correspond to the kinetic parameters that are defined by the biomolecular recognition event. For affinity sensors used in quantification, the ideal highly sensitive detection is one where the majority of the analyte is uniformly associated and transported to the affinity sensor surface.

Recently, there has been much effort focused on the reduction of the size of these integrated affinity sensor devices [7]; this provides i) the potential to use arrays of parallel sensors for the quantification of multiple analytes simultaneously [8, 9], ii) reduced sample volumes and iii) approaches for more sensitive detection and rapid analysis times [10]. While there has been significant effort focused on a reduction of the sensor size [11], far less attention has been placed on improvement of the design of the microfluidic elements of the integrated system. This is a very important design consideration, especially where the sensor size and/or analyte volume is small and where optimum, highly sensitive levels of detection are needed. Indeed advantages achieved in sensor sensitivity will be fruitless if strategies to incorporate improved analyte transport are neglected.

Typically, transport of the analyte to the sensor in an integrated microfluidic device is dominated by molecular diffusion within a stable laminar flow. Because diffusion is the only method for delivering the analyte to the recognition molecules on the sensor surface, the replenishment of the analyte at the sensor surface is subject to mass transport limitations, as elegantly demonstrated by Caelen et al. [12] and Goldstein et al. [13]. However, several mechanical and

physical strategies have been implemented to achieve more efficient transport of the analyte to the sensor surface, some of the most effective are based upon methods for mixing of the analyte within the flow chamber by incorporating a passive or active micromixer [14, 15]. For example Abrantes et al. [16] demonstrated that, by periodically pulsing the analyte solution in a 'forward-backward' flow in serpentine channels, higher yields of analyte could be measured on the sensor patches. Vijayendran et al. [17] demonstrated that the integration of three-dimensional serpentine channels, which are passive mixers, would improve the yield of analyte detected at the sensor. In a recent study [18], a channel with slanted groove/herringbone ridges patterned in the top of the channel [19] was combined with a microfluidic sensor, this approach provided much better analyte detection limits, with an improvement of 26-46%. An innovative active mixer strategy has been reported by Jennisen and Zumbrink, where a bubble was introduced into the channel in front of the analyte fluid. The bubble was moved over the sensor through the fluid and this created a 'mixing' vortex sheet between a fluid layer close to the sensor surface and the bulk analyte fluid [20]. This simple, but innovative approach resulted in very good transport of the analyte to the sensor surface and effective mixing.

While some effort has been focused on improved mixing and transport of the analyte to the sensor surface, all these systems are designed for conditions where sufficient volumes of analyte fill the channel. More often than not the volume of analyte is limited and this needs to be injected as a short 'plug' (the case considered below in this paper). Little design consideration has been given to the effects of depletion of the sample as it moves along the channel over the affinity sensor. For channel heights in the low micrometer range and a small

analyte plug, the depletion of the analyte in the bulk flow becomes significant [21]. The resulting analyte association to the active area of the affinity sensor is non-uniform and this can lead to a less robust and sensitive integrated affinity sensor system. This is particularly true for fluorescence based sensor systems where high concentrations of fluorescently labelled analyte are prone to quenching [22] and the yield of emission from the fluorophores is non-linear with the absorption cross-section of the excitation light.

In this paper new microfluidic approaches and designs are considered where both high yield and uniform association of the analyte over the affinity sensors are provided. These simple designs and strategies for a microfluidic flow channel will lead to an improved sensor response. The design is suitable for use with small volumes of reagent on small scale sensor devices. This is becoming increasingly important with the requirement for multiplex analysis of small samples of biological origin.

2 Theoretical Model

The theoretical model, used both to establish the mass transfer of the analyte to the affinity sensor from the bulk flow in the microchannel and to maintain the uniformity of the associated analyte bound to the recognition molecules, for both (i) integrated microfluidic channels conventionally used with affinity sensors and (ii) optimised fluidic - affinity sensor formats, is presented here. The aim in this work is not to create a highly specialized mathematical model of a specific analyte system, but rather to create approaches that contain the main elements of the physical system and that can be easily exploited to identify and understand the optimal conditions for an integrated affinity -

microfluidic sensor design and usage.

Analytes in microfluidic affinity biosensors are transported by pressure driven flow over a stationary affinity sensor. The predominant processes, which dictate the behaviour of the analyte, include molecular diffusion and convection as well as binding to recognition molecules on the sensor surface. A schematic representation of a fluidic channel and integrated affinity sensor, showing the active area, along with the corresponding co-ordinates and dimensions, is given in Figure B.1.

The transport of analytes in the fluid is described using the established equation [23]

$$\frac{\partial [\mathrm{A}]}{\partial t} + \vec{u} \cdot \nabla [\mathrm{A}] = D \Delta [\mathrm{A}] \tag{1}$$

where [A] is the concentration of the analyte, $\vec{u}$ is the flow velocity and D is the constant diffusion coefficient. The behaviour of the analyte molecules in the fluidic channel is described by convective transport of the analytes in the fluid flow and molecular diffusion. The analytes are to be transported by pressure driven flow, and the flow velocity is governed by the Navier-Stokes equations. The small characteristic length of microfluidic channels provides a small Reynolds number [24] and this dictates that viscous effects dominate over inertia effects. So the inertia terms in the Navier-Stokes equations are neglected [25] and a stable laminar flow profile is obtained.

For the recognition process on the sensor surface, the simplest, $1:1$ analyte to recognition molecule binding event is considered. In addition the model is restricted to irreversible association or where the rate of dissociation is so slow that it can be neglected.

$$A + X \xrightarrow{k_a} B$$

where the analyte A binds to the immobilised active recognition binding site X to form the recognition molecule-analyte complex B. The constant k_a is the rate constant for the bimolecular reaction between the analyte and the recognition molecules. By the law of mass action, the rate of formation of the complex B on the sensor surface is

$$\frac{\partial [\mathrm{B}]}{\partial t} = k_a [\mathrm{A}] |_s [\mathrm{X}] \tag{2}$$

where [X] and [B] are the sensor surface concentration of the free and occupied recognition molecule sites, respectively, and $[\mathrm{A}] |_s$ is the value of [A], the volume concentration in the fluid, at the surface. In addition, each surface attached recognition molecule is either occupied by an analyte molecule or free, so that

$$[\mathrm{B}] + [\mathrm{X}] = [\mathrm{X_0}] \tag{3}$$

where $[\mathrm{X_0}]$ is the total concentration of recognition molecules.

It is assumed that, i) the laws of mass conservation apply, ii) the transfer of analyte from the bulk solution to the sensor surface is purely by diffusion and convection, iii) there is no initial surface concentration of analyte associated on the active area of the sensor and iv) the transfer of analyte from the fluid is balanced by the rate of analyte association on the active area. Hence at the active surface of the sensor

$$D \left. \frac{\partial [\mathrm{A}]}{\partial y} \right|_s = \frac{\partial [\mathrm{B}]}{\partial t} \tag{4}$$

From the equations 2 , 3 and 4 it follows that

$$\frac{\partial [\mathrm{A}]}{\partial y} = \frac{k_a}{D} [\mathrm{A}] |_s ([\mathrm{X_0}] - [\mathrm{B}]). \tag{5}$$

Equation 5, together with equation 4, forms the boundary conditions for equa-

tion 1 on the active surface; the additional boundary conditions include no movement of analyte across non-active channel walls ($[\mathrm{A}]_y = 0$ and $[\mathrm{A}]_z = 0$) and no diffusive movement of analyte across the channel exit ($[\mathrm{A}]_x = 0$) (here $[\mathrm{A}]_y = \partial [\mathrm{A}] / \partial y$ has been introduced as a shorthand notation).

In contrast to much of the published theoretical work in this field [26, 5], a continuous analyte input is not used. Instead, an analyte 'plug' is injected in a pulse of time, λ, so that at the entrance to the channel

$$[\mathrm{A}](0, y, z, t) = [\mathrm{A}_0]\, H(t) H(\lambda - t) \tag{6}$$

where $[\mathrm{A}_0]$ is the initial concentration of the analyte and H is the Heaviside function.

To gain insight into the behaviour of the mathematical model, the governing equations and boundary conditions are nondimensionalised with the following variables: $x = L\bar{x}$, $y = H\bar{y}$, $z = W\bar{z}$, $[\mathrm{A}] = [\mathrm{A}_0]\,[\bar{\mathrm{A}}]$, $[\mathrm{X}] = [\mathrm{X}_0]\,[\bar{\mathrm{X}}]$, $[\mathrm{B}] = [\mathrm{X}_0]\,[\bar{\mathrm{B}}]$ and $t = \frac{L}{U}\bar{t}$, where U is the mean velocity of the flow through the channel. (Other feasible nondimensionalisation approaches are also possible and have been applied for different analysis problems, where they are better suited [21, 27].) In this case the resulting problem is :

$$[\bar{\mathrm{A}}]_{\bar{t}} + \vec{\bar{u}} \cdot \nabla [\bar{\mathrm{A}}] = \frac{LD}{UH^2} \left(\frac{H^2}{L^2} [\bar{\mathrm{A}}]_{\bar{x}\bar{x}} + [\bar{\mathrm{A}}]_{\bar{y}\bar{y}} + \frac{H^2}{W^2} [\bar{\mathrm{A}}]_{\bar{z}\bar{z}} \right) \tag{7}$$

$$[\bar{\mathrm{A}}]_{\bar{y}}\Big|_s = \frac{k_a H\,[\mathrm{X}_0]}{D}\; [\bar{\mathrm{A}}]|_s (1 - [\bar{\mathrm{B}}]) \tag{8}$$

$$[\bar{\mathrm{B}}]_{\bar{t}} = \frac{D[\bar{\mathrm{A}}]_0 L}{H[\bar{\mathrm{X}}]_0 U}\; [\bar{\mathrm{A}}]_{\bar{y}}\Big|_s . \tag{9}$$

(For the ease of readability the bar atop the nondimensional variables is neglected from now on.)

For most microfluidic channels the height is much smaller than the width and length. It is therefore reasonable to neglect the diffusion in the x and z direction, as $H/L \to 0$ and $H/W \to 0$. In addition, it is only considered that analyte is introduced in short pulses into the channel and hence it is assumed that $\lambda U/L$ is small.

There are then two central nondimensional parameters, the Graetz number, Gz and the Damköhler number, Da. These are defined as:

$$\begin{aligned} \mathrm{Gz} &:= \frac{H^2 U}{LD} = \frac{\text{diffusion time}}{\text{residence time}} \\ \mathrm{Da} &:= \frac{k_a H \left[\mathrm{X}_0\right]}{D} = \frac{\text{binding rate}}{\text{diffusion rate}}. \end{aligned}$$

The Graetz number, Gz is a measure for the relative importance of diffusion and convection. For $\mathrm{Gz} \ll 1$ all analyte molecules have enough time to diffuse to the recognition molecules attached on the surface of the sensor. As a consequence, the concentration profile is fully developed, while for $\mathrm{Gz} \gg 1$ many analyte molecules flow through the device without encountering the recognition molecules on the sensor surface and the channel is said to be in the 'entrance region'. The Damköhler number, Da, relates the rate of transport to the recognition molecules on the surface to the rate of binding. For $\mathrm{Da} \ll 1$ the rate of binding is much slower than diffusion and the system is said to be binding limited, while for $\mathrm{Da} \gg 1$ the diffusion is much slower than the rate of binding and the system is diffusion limited.

A third important nondimensional parameter is the relative adsorption capacity, κ, defined by

$$\kappa := \left[\mathrm{X}_0\right] / \left[\mathrm{A}_0\right] H$$

which describes the relationship between the recognition molecule concentra-

tion and the bulk concentration.

For the sensor applications of interest here, where small samples are used, the devices are designed such that a large adsorption capacity value applies. To achieve this it is assumed that the recognition molecules attached on the sensor surface are at a high concentration and the total available is far in excess of the amount of analyte. The concentration will remain almost constant, at $[X_0]$, throughout the measurement, thus every analyte molecule reaching the sensor surface has the same opportunity to bind to a recognition molecule.

This model is now used to optimise the behaviour of integrated affinity sensors with respect to two quantities, namely the spatial uniformity of the analyte, and the fraction of analyte associated to recognition molecules on the sensor surface.

The numerical calculations are done with the PDE package COMSOL Multiphysics 3.2 (COMSOL AB, Stockholm, Sweden) and with MATLAB 7.1 (The Mathworks, Natick, MA, USA).

3 Rectangular channel with constant parameters

In the first instance the theoretical performance of the reported integrated microfluidic - multisensor system of Hua et al. [2] was evaluated. Although this system has an excellent detection limit, below $1ng/l$ for estrone, the design of the microfluidic elements had not been optimised. For this study, the dimension of the theoretical model is reduced by assuming that the analyte transport and association on the active area is uniform over the complete width of the device. For the multisensor channel of Hua et al., where the width, W, is about

140 times the height, H, this is a sensible assumption as 3D effects would only be important very close to the side wall boundaries. This reduction of the governing equation 7 leads to the following equation,

$$[\mathrm{A}]_t + u\,[\mathrm{A}]_x = \frac{1}{\mathrm{Gz}}\,[\mathrm{A}]_{yy} \tag{10}$$

where the velocity, u is only dependent on the channel height and represents the parabolic flow profile.

The diffusion coefficient for small molecules and many proteins is of the order of $5 \cdot 10^{-11} m^2 s^{-1}$ [28]. The multisensor of [2] is $35\mu m$ high and every sensor patch is $1.5mm$ long. The average flow velocity is $14mms^{-1}$ which yields a Graetz number of 228. The sensor clearly operates in the 'entrance region' and less than 10% of the analyte molecules reach the affinity sensor surface to bind to recognition molecules. For many antibody-antigen interactions k_a is between $1 \cdot 10^5$ to $8 \cdot 10^5$ Ms^{-1} [29]. With a receptor concentration $[\mathrm{X}_0] = 7 \cdot 10^{-8} molm^{-2}$ a Damköhler number of between 5 and 40 is estimated: the system is diffusion limited. Figure B.2 illustrates the expected result for a continuous analyte input, where the analyte concentration contours are shown: the majority of the analyte molecules flow through the device without encountering recognition molecules on the sensor surface and the analyte molecules that reach the surface, bind almost immediately. This means that a large amount of the analyte will travel through the integrated fluidic-sensor device and will be undetected. Simulations performed with an analyte pulse of $1s$ and a rate constant $k_a = 8 \cdot 10^5 Ms^{-1}$ show that less than 5% of the analyte will be bound by the receptor molecules on the surface. Such a configuration might be appropriate to establish the rate constant for the physical interaction between the analyte and the recognition molecule attached to the affinity

sensor, for instance in a Biacore sensor [30]. However, where highly sensitive quantification of analytes is the aim, then an alternative strategy for analyte handling is required.

The first step to improve the system would be to provide a strategy to increase the fraction of analytes that travel to the recognition molecules on the sensor surface. A further reduction in channel height and fluid flow velocity are the most feasible options to reduce the Graetz number. The integrated device operates in the, so called, fully developed region. The concentration of analyte associated on the affinity sensor, in the fully developed region, is dependent on the reaction rate constant. For analytes with high rate constants, almost 100% binding of analyte would be expected. This high yield comes at the expense of the uniformity of the analyte associated over the sensor surface; a large fraction of the analyte is bound by recognition molecules at the 'front' of the affinity sensor patch, over which the analyte plug first travels. For slower reactions less analyte is associated and this results in non-depleted analyte plugs. The slower the reaction the better is the uniformity of the sensor-associated analyte, but less analyte is associated in total. Whilst the model can be used to define the optimal flow rate and channel height for high levels of bound analyte on the affinity sensor, there is not a straight-forward method to achieve both high and uniform analyte association. Design concepts, to achieve this for affinity sensors in integrated microfluidic systems, are now considered as well as fluidic channel geometries and protocols to offset the decrease in plug concentration of the analyte along the channel.

4 Design optimisation

Highly sensitive small scale affinity sensors are of limited value without consideration of the microfluidic elements for analyte transport. Optimal sensor response will be obtained by achieving, i) a uniform coverage of the affinity sensor with analyte and ii) high yields of analyte associated on the affinity sensor surface. Approaches investigated include those that exploit the fluid flow speed, the density of the recognition molecules on the active area and finally, the most simple practically realistic solution, new designs of the microfluidic channels. Only fully developed systems where the Graetz number is much smaller than 1, a 'binding limited system', are considered.

4.1 Fluid flow speed

The first scenario considered is where the flow rate of the analyte, through the channel over the affinity sensor, is reduced as it travels over the active surface. For the case with a small Graetz number, the analyte plug concentration, [A] is considered to be constant across the channel height. Thus [A] depends only on the distance along the channel, x and time, t. This analyte plug moves along the channel with the average flow velocity. The equation 10 is integrated over the height of the channel and equation 8 is used to yield

$$\frac{\partial [\mathrm{A}]}{\partial t} + u(t)\frac{\partial [\mathrm{A}]}{\partial x} = -\frac{1}{H}\frac{k_a L [\mathrm{X_0}]}{U}[\mathrm{A}](1-[\mathrm{B}]) \tag{11}$$

$$\frac{\partial [\mathrm{B}]}{\partial t} = \frac{k_a L [\mathrm{A_0}]}{U}[\mathrm{A}](1-[\mathrm{B}]) \tag{12}$$

where $[\mathrm{A}](x,t)$ is the average concentration in the channel, U is the initial velocity and $u(t)$ describes the variation from the initial velocity ($u(0) = 1$).

From equation 12, the bound concentration, [B] can be determined in terms of the bulk concentration [A]

$$[\mathrm{B}](x,t) = 1 - \exp\left(-\int_0^t \frac{k_a L\,[\mathrm{A}_0]}{U}\,[\mathrm{A}](x,t)dt\right). \tag{13}$$

For systems with a large relative absorption capacity, κ, [B] is small and thus can be ignored in equation 11. In these circumstances [A] is now independent of the surface site concentration, thus the behaviour is described by a travelling wave where the height is only dependent on the time it needs to reach the point x

$$\begin{aligned}[\mathrm{A}](x,t) = {} & e^{-\alpha(t-t_1)} H\left(\int_0^t u(t)dt - x\right) \\ & H\left(x - \int_\lambda^t u(t)dt\right)\end{aligned} \tag{14}$$

with t_1 defined by the equation $\int_{t_1}^t u(t) = x$. The nondimensional binding/convection number, α, is

$$\alpha = \frac{\mathrm{Da}}{\mathrm{Gz}} = \frac{k_a L\,[\mathrm{X}_0]}{HU} = \frac{\text{binding rate}}{\text{convection rate}}. \tag{15}$$

The capture fraction, F, of analyte can be calculated through $F := 1 - exp(-\alpha)$ and thus for a high binding/convection number, α, a yield of bound analyte of almost 100% will be achieved. Having determined the analyte concentration, [A], as determined in equation 14, this can be inserted into equation 13 and be used to establish how best to moderate the flow rate of the analyte plug over the affinity sensor to obtain a constant value for the bound analyte [B] over the affinity sensor active area. In this case, this is equivalent to seeking

$$\int_0^T [\mathrm{A}](x,t)dt = const \tag{16}$$

for all values of x and for T sufficiently large. (Note that this approximation will break down if $[\mathrm{A}_0]$ is so high that the condition of a large relative

absorption capacity is invalid.)

The variation of flow speed with time $u(t)$ that makes equation 16 valid is sought. The variable flow speed for $0 \leq t \leq T$ is established by using the approximation

$$u(t) = exp(-at) \tag{17}$$

where a is a free parameter and a least-square optimisation is performed. This is a natural and very robust approach to compensate for the exponential decrease of the analyte concentration. The optimal condition is where the flow speed is gradually reduced as the analyte plug passes over the affinity sensor; thus there is more time for the analyte to bind as the plug concentration depletes along the active area.

Figure B.3 contains plots of the simulated results for the rectangular channel where the flow speed of the analyte plug over the sensor is constant (section 3) and that for the optimised variable flow speed obtained using the approach described here. The density of analyte associated over the length of the affinity sensor is almost uniform and the amount of analyte associated is greater than for the constant case (section 3). Although an approximate model was used for the optimisation, where the large absorption capacity was exploited, these simulations have been performed with a full 1D model including diffusion and the reduction of surface site concentration. Thus the simplifications used are reasonable.

Up to a value of around $\alpha = 0.7$ this approach gives a very uniform surface coverage and also a large increase in the capture fraction. For $\alpha = 0.7$ about 75% of the analyte is captured at the active surface which is an improvement of about 50% over the constant flow speed case. For larger values of the

nondimensional binding/convection number, α this optimization still yields a uniform density of bound analyte over the majority of the affinity sensor, however the density drops dramatically at the last part of the active area. The ansatz u is not flexible enough to counter the near complete depletion of the analyte plug under these conditions. To achieve uniform analyte coverage on the affinity sensor, for this case, a more complex and powerful representation of the flow speed is needed.

4.2 Recognition molecule concentration

The second approach considered (for microfluidic sensor design optimisation) was the distribution of recognition molecules over the active area of the sensor. More specifically, how a variation in the density of these covalently attached molecules along the active area of the sensor can be exploited to result in uniform yields of associated analyte over the active area of the sensor.

The total receptor concentration is taken to be $[\mathrm{X_0}]\,[\mathrm{X_s}](x)$ where $[\mathrm{X_0}]$ is the concentration at the outlet and $[\mathrm{X_s}](x)$ describes the variation of density of recognition molecules attached along the active area of the sensor ($[\mathrm{X_s}](1) = 1$). By increasing the density of covalently attached recognition molecules along the sensor surface it may then be possible to achieve a uniform density of associated analyte after an analyte plug has been passed over it. For these studies the flow velocity of the analyte is constant.

A similar analysis, as in section 4.1, results in equations describing the analyte, [A], and the associated analyte, [B], as a function of distance along the channel, x, and time, t.

$$[\mathrm{A}](x,t) = \exp\left(-\alpha \int_0^x [\mathrm{X_s}](x)dx\right) H\left(t-x\right) H\left(x-t+\lambda\right) \tag{18}$$

$$[\mathrm{B}](x,t) = [\mathrm{X_s}](x)\left(1-\exp\left(-\lambda\frac{\alpha}{\kappa}[\mathrm{A}](x,t)\right)\right) \tag{19}$$

In this case it is necessary to optimise over the whole expression and seek the function $[\mathrm{X_s}](x)$ so that

$$[\mathrm{B}](x,t) = const \tag{20}$$

for all x and for t sufficiently large. Again a least-squares optimisation is used with the following object function

$$[\mathrm{X_s}](x) = exp(-a(1-x)). \tag{21}$$

In the first example, described in section 3, the concentration of surface attached recognition molecules, attached at the sensor at the channel exit and entrance, is constant. To achieve a more uniform association of analyte over the sensor surface, a lower density of recognition molecules is covalently attached to the front of the active area of the sensor over which the analyte will first traverse. The density of the attached recognition molecules increases across the active area of the sensor. For the purposes of our study, the density of surface attached recognition molecules at the exit is considered to be the same as for the system considered in section 3. Thus the model provides a spatial limitation for the rate of association of the analyte with the recognition molecules as a function of the position over the sensor.

Figure B.4 shows simulation results for the full 1D model. Under these conditions the density of analyte, associated over the whole length of the active surface, is constant. As expected, the total analyte yield that is associated is lower than for the case where the active area is patterned with a uniform den-

sity of recognition molecules (at the maximal density of the former case). Thus as expected, the ansatz 21, used to establish the density gradient of recognition molecules over the active surface of the sensor, leads to a reduction in the number of available binding sites. The reduction of the concentration of recognition molecules, $[X_0]\,[X_s](0)$ at the channel entrance leads automatically to a reduction of α. Thus even systems with analytes having high rate constants for the reaction with the recognition molecules can be optimised.

Equation 19 can be used to evaluate the impact of input concentration of the analyte, $[A_0]$, on the required recognition molecule density on the surface. The optimal surface site concentration was calculated for a single input concentration $[A_0]$, these results were then used to examine the effect of different analyte input concentrations on the surface coverage of associated analyte over the sensor. For lower input concentrations, there was no visible effect on the uniformity of the associated analyte density. The same is true for higher concentrations of up to 10 times the initial input analyte concentration. However, if even higher concentrations are used the approach fails because the prerequisite of a high capacity system is violated.

4.3 Channel shape and active area

A more practical solution, as compared to the approaches discussed in sections 4.1 and 4.2, is the utilisation of a non-rectangular channel and active area to increase the transport of the analyte to the recognition molecules attached to the active area of the sensor. The design for the channel will firstly be non rectangular and secondly have a sensor active area, with a uniform density of recognition molecules, in the lower surface of the channel.

Figure B.5 shows a birds-eye view representation of a tapered channel, assumed to be of constant height, and with the parameter conventions indicated. The lower surface is divided into a region with no recognition molecules (shown in white) and a region with uniform recognition molecules attached to the active area (shown in grey). Different geometries of the channel ($W(x)$)and shapes for the active area of the sensor on the base of the channel ($g(x)$) are considered. A tapered channel is used, and thus streamlines shown in the figure represent the analyte in the bulk flow that crosses from the peripheral edges of the channel over the active area of the sensor. Utilisation of a channel and integrated sensor of this geometry provides continuous replenishment of analytes to the active area along the channel; this was considered to offer the advantage of reducing the effects of depletion of the analyte concentration in the bulk, due to binding with recognition molecules on the active area.

For this case, the following equation describes the temporal variation of the analyte concentration in the channel: taking into account the convection with the flow and the binding of the analyte to the recognition molecules on the active area of the sensor.

$$\frac{\partial [\mathrm{A}]}{\partial t} + u [\mathrm{A}]_x + w [\mathrm{A}]_z = -\chi(x,z)\frac{1}{H}\frac{k_a L [\mathrm{X_0}]}{U} [\mathrm{A}](1 - [\mathrm{B}])$$

with the active region described by $\chi(x,z) = 1$ for $0 \leq z \leq g(x)$ and zero otherwise. In solving the problem we shall assume that the channel is symmetric and hence only show the region $0 \leq z \leq W(x)$.

The system, compared to the previous ones (section 4.1 and 4.2), has the added complexity that the fluid velocity in both the x and z directions must be considered. However, by using the appropriate thin film theory [25], the velocity is dependent only on the gradient of the pressure. As a result of

mass conservation, the pressure, p, obeys the Laplace equation. The boundary conditions are then $p = c_1$, $p = c_2$, $p_z = 0$ and $p_n = 0$ at the channel entrance, channel exit, the middle of the channel and the channel wall, respectively.

Microfluidic channels with tapering regions were used as a starting point for these studies; these channels are defined through the solutions $p_1 = z^2 - x^2$ and $p_2 = \log(x^2 + z^2)/2$ to the Laplace equation. To fulfil the boundary conditions, the channel side wall geometries are matched with the orthogonal trajectories of the pressure isobars in the channels, and this thus defines the dimensions of the channel entrance and exit. The pressure, p_1, defines a channel with an exponential decrease in width, while p_2 defines a channel with a linear decrease in width, as indicted in figure B.6. The only difference between these two channel structures, as compared with the originally proposed channel (figure B.5), is at the channel entrance and exit, which are no longer straight lines. The deviation resulting from a difference in a vertical inlet and outlet, compared to the shaped ones, will only have a small effect on the resulting flow velocity. These two different channel designs provide enough flexibility to evaluate how the tapering geometry of the channel impacts on the yield of analyte that is transferred from the bulk fluid flow to the active area of the sensor.

Optimisation of the design of both the channel and the shape of the active area of the sensor would require a full numerical evaluation, but this was not likely to provide sufficient insight to be valuable. Thus a simplified approach was taken. Rather than optimising both, the shape of the channel, $W(x)$, is fixed and only the optimal shape of the active area, $g(x)$, is established theoretically. The objective is to achieve a high yield and uniform density of associated analyte on the active surface. Thus, to a first approximation, a

uniform flux of analyte across the active/inactive interface along the channel is required.

The active/inactive interface is defined as $g(x)$ and the conditions, that the active/inactive interface leaves a clear channel opening, $g(x = 0) = 0$ and extends across the entire channel at the exit $g(x = 1) = W(x = 1)$, are imposed. The approximate optimisation problem is formulated in the following way. The active/inactive interface, $g(x)$, is determined such that

$$\mathbf{u} \cdot \mathbf{n}_g = const \tag{22}$$

where $\mathbf{u}$ is the flow velocity at the interface and $\mathbf{n}_g$ is the normal to the interface g. With the analytic description of the flow speed determined from the pressure fields, this leads to an ordinary differential equation for $g(x)$. MATLAB 7.1 is used to solve this non-linear boundary value problem numerically. The solutions for two channels, defined through the pressure fields $p_1 = z^2 - x^2$ and $p_2 = \log(x^2 + z^2)/2$, are given in figure B.6.

To establish whether the approximations made here were reasonable, simulations using the full 2D model, including diffusion in the x and z direction, were performed on the optimal interface shapes, that had been identified and shown in figure 6. Simulation results from these calculations are shown in figure B.7.

In assessing the uniformity of the analyte, associated on the active area, the following integral was used

$$\text{Uniformity} = \frac{\int_S ([\text{B}](x,z) - [\text{B}]_{mean})^2 \, dz \, dx}{[\text{B}]_{mean}^2 \int_S dz \, dx}$$

where S is the active surface and $[\text{B}]_{mean}$ is the average bound concentration.

Thus the analyte will be more uniformly bound over the sensor, as compared

to the integrated system described in section 3. The resulting improvement of the uniformity, for a system with $\alpha = 0.9$, is about 25% compared to a conventional channel from section 3. For higher values of α the improvement is higher. This is due to the faster depletion of the bulk concentration so that the analyte replenishment is more effective. There is a clear trade-off between the tapered channels here and the straight channel system described in section 3. In straight channels with the same reaction/convection number up to twice as much of the analyte associates on the affinity sensor. The reason for this is that the time where the bulk solution is not above the active area is 'lost time for binding'. It is therefore not surprising that a large fraction of the analyte is not captured by the recognition molecules over the active area, this loss is particularly true at the edges of the tapered channels. The difference in capture fraction, between straight and tapered channels, decreases with increasing reaction/convection number, α.

The major advantage for integrating tapered channels over the straight channels in affinity sensors is that multiple affinity sensors in series can be used. For these tapered fluidic channels, the amount of analyte associated on the active surface is dependent on the average flow velocity. Differences in the rate constant for the association, k_a, can be balanced by different average flow velocities to yield the same level of association for different sensor elements. By moderating the inlet-to-outlet size ratio, the average flow velocity can be changed while still maintaining the flow rate over the whole system as constant. By increasing the inlet-to-outlet ratio from 1.5 to 4.5 the attachment level is decreased by a factor of 1.85. Thus for a series of sensors for the detection of multiple analytes, the channels can be tailored to suit the binding properties of the analyte-recognition system.

5 Conclusion

To date, little consideration for both efficient and uniform mass transfer of the analyte to the affinity sensors had been made. When microfluidic channels are operated in the fully developed region, the depletion of the analyte plug plays a significant role in the analyte association at the active surface. Here theoretical models have been created for optimal integrated affinity sensor design, whereby both uniform association of analyte and high yield of mass transfer to the active area of affinity sensors could be achieved. This has been achieved by consideration of flow speed, recognition molecule concentration and channel shape design. Each system has specific advantages. A reduction of the flow of an injected analyte plug over the affinity sensor in a rectangular channel provides the most effective method for both providing efficient mass transfer and uniformity of the analyte bound to the sensor surface, and this is almost irrespective of the analyte concentration. An increase of the recognition molecule concentration along the channel provides a stable method to achieve a uniform association of analyte molecules. The application of tapered fluid channels over the affinity sensor would provide the simplest practical approach for transport of analyte to the active area of the sensor. Here the analyte will be delivered to the active area in such a way that the resulting associated analyte will be uniform over the affinity sensor. Furthermore these tapered structures could be designed for a series of different analyte - recognition molecules on different affinity sensors in series, thus tailoring each system for the most efficient and effective detection of the analyte. Such a strategy has not been previously reported.

A Implementation and validation of the model

The governing equations are implemented in COMSOL Multiphysics 3.2 (COMSOL AB, Stockholm, Sweden) to carry out the numerical simulations. The dimension of the full 3D, dimensional convection-diffusion equation 1 is reduced along the lines of section 4.1 to yield the 2D transport-reaction equation

$$\frac{\partial [\mathrm{A}]}{\partial t} + u\frac{\partial [\mathrm{A}]}{\partial x} + w\frac{\partial [\mathrm{A}]}{\partial z} = -k_a [\mathrm{A}](1 - [\mathrm{B}]) + D\left(\frac{\partial^2 [\mathrm{A}]}{\partial x^2} + \frac{\partial^2 [\mathrm{A}]}{\partial z^2}\right) \quad \text{(A.1)}$$

$$\frac{\partial [\mathrm{B}]}{\partial t} = k_a [\mathrm{A}](1 - [\mathrm{B}]) \quad \text{(A.2)}$$

In COMSOL Multiphysics, equation A.1 is defined as a 'Convection and Diffusion' model while equation A.2 is modelled through the 'Diffusion' model. Both models are linked through the reaction rate $k_a [\mathrm{A}](1 - [\mathrm{B}])$ which is defined as a 'Subdomain Expression'. The temporal variable speed and spatial variable recognition molecule concentration, from subsections 4.1 and 4.2, are defined as 'Functions' dependent on t and x, respectively. The flow speed, w, in the z direction is zero except for the non-rectangular channels in subsection 4.3. The first calculations are then performed with the mesh COMSOL generates automatically.

A comparison of the results for the numerical simulation with an analytical approximation for equation 10, in the case of fast vertical diffusion, shows very good agreement between the two solutions. In addition, we performed a mesh convergence test where we compared the results for a coarse mesh with the next finer, predefined, mesh size of COMSOL to deduce the necessary mesh size. We also compared the analytic analyte input with the numerical analyte input to find an upper boundary for the time stepping.

Acknowledgements

We are grateful for the financial support of the EPSRC and the BBSRC. We also acknowledge the valuable contributions of Prof. J. Wilkinson and Mrs. P. Hua (ORC, University of Southampton).

B Figures

Fig. B.1. Schematic diagram of an integrated microfluidic affinity sensor

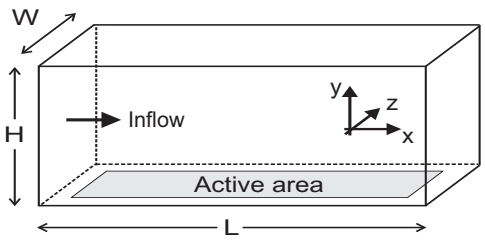

Fig. B.2. Simulated bulk concentration for one sensor patch of the multisensor [2]. Contours of the analyte concentration are shown. Parameters: $H = 35\mu m$, $W = 5mm$, $L = 1.5mm$, $U = 14mms^{-1}$, $[\mathrm{X}_0] = 7 \cdot 10^{-8} molm^{-2}$, $[\mathrm{A}_0] = 0.1\mu M$, $k_a = 8 \cdot 10^5 Ms^{-1}$

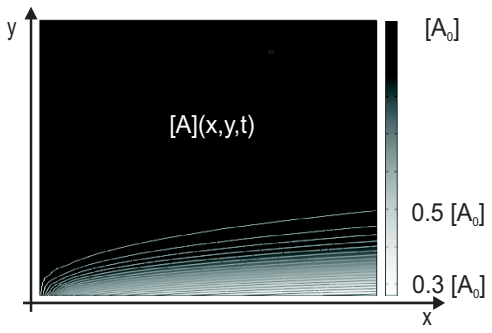

Fig. B.3. Simulation results for a rectangular microfluidic channel for constant flow rate (dashed line) (as described in section 3) and optimised flow rate (solid line). Parameters: $H = 10\mu m$, $W = 1.5mm$, $L = 1.6mm$, $U = 1mms^{-1}$, $[\mathrm{X}_0] = 1 \cdot 10^{-8} molm^{-2}$, $[\mathrm{A}_0] = 0.1\mu M$, $k_a = 2.4 \cdot 10^5 Ms^{-1}$

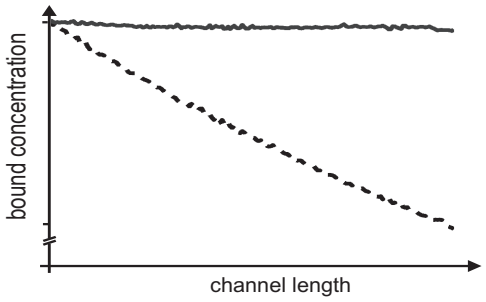

Fig. B.4. Simulation results for a rectangular microfluidic channel for constant surface site concentration (solid line) and optimised surface site concentration (dashed line). The diagram shows the impact of applying the analyte over a sensor with a non-constant surface site concentration: the analyte is associated in a more uniform way over the sensor. Parameters: $H = 10\mu m$, $W = 1.5mm$, $L = 1.6mm$, $U = 1mms^{-1}$, $[\mathrm{X}_0] = 1 \cdot 10^{-8} molm^{-2}$, $[\mathrm{A}_0] = 0.1\mu M$, $k_a = 2.4 \cdot 10^5 Ms^{-1}$

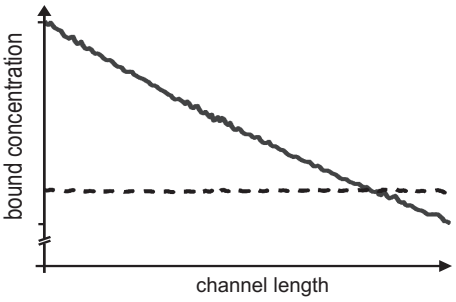

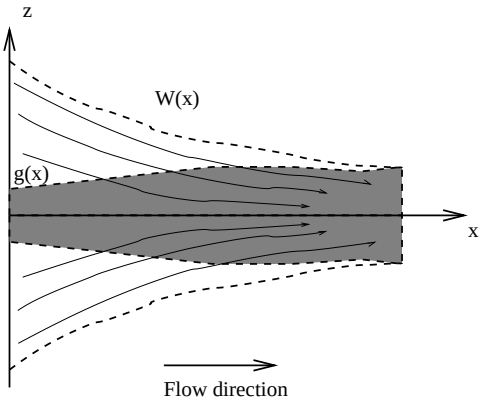

Fig. B.5. A plan view of a channel with decreasing width showing the geometry and the streamlines. The edge of the channel is $W(x)$ while $g(x)$ is the curve separating the region on the lower surface where there are active recognition molecules (shown in grey) from the inactive region shown in white).

Fig. B.6. Tapered channels which have very simple pressure distributions. Top: Channel design and optimal sensing area for $p_1 = z^2 - x^2$. Bottom: Channel design and optimal sensing area for $p_2 = \log(x^2 + z^2)/2$. The optimal $g(x)$ found using the approxiamte method is also shown

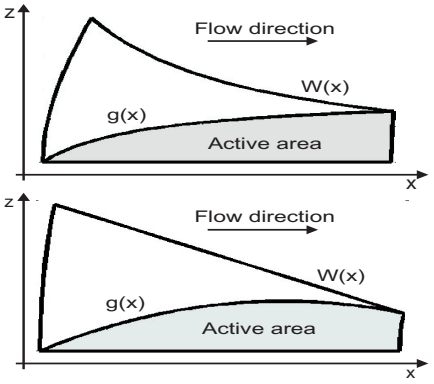

Fig. B.7. Simulation results showing the contours of the bound concentration, [B] for the optimised channels after the analyte plug has exited the channel. Parameters: $H = 10\mu m, W(0) = 0.5mm, L = 1.6mm, U = 2mms^{-1}, [\mathrm{X}_0] = 1 \cdot 10^{-8} molm^{-2}$, $[\mathrm{A}_0] = 0.1\mu M, k_a = 2.4 \cdot 10^5 Ms^{-1}$

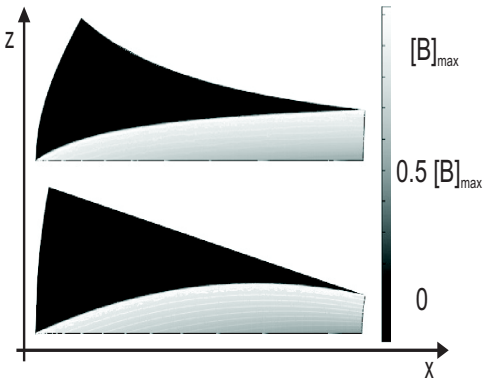

References

[1] S. Rodriguez-Mozaz, M. J. L. de Alda, D. Barcelo, Biosensors as useful tools for environmental analysis and monitoring, Anal. Bioanal. Chem. 386 (4) (2006) 1025–1041.

[2] P. Hua, J. P. Hole, J. S. Wilkinson, G. Proll, J. Tschmelak, G. Gauglitz, M. A. Jackson, R. Nudd, H. M. T. Griffith, R. A. Abuknesha, J. Kaiser, P. Kraemmer, Integrated optical fluorescence multisensor for water pollution, Opt. Express 13 (4) (2005) 1124–1130.

[3] D. Altschuh, S. Oncul, A. P. Demchenko, Fluorescence sensing of intermolecular interactions and development of direct molecular biosensors, J. Mol. Recognit. 19 (2006) 459–477.

[4] J. Homola, S. S. Yee, G. Gauglitz, Surface plasmon resonance sensors: review, Sens. Actuators, B 54 (1-2) (1999) 3–15.

[5] A. Önell, K. Andersson, Kinetic determinations of molecular interactions using biacore - minimum data requirements for efficient experimental design, J. Mol. Recognit. 18 (4) (2005) 307–317.

[6] V. Sikavitsas, J. M. Nitsche, T. J. Mountziaris, Transport and kinetic processes underlying biomolecular interactions in the biacore optical biosensor, Biotechnol. Prog. 18 (4) (2002) 885–897.

[7] J. C. T. Eijkel, A. van den Berg, Nanofluidics: what is it and what can we expect from it?, Microfluid. Nanofluid. 1 (3) (2005) 249–267.

[8] B. B. Haab, Applications of antibody array platforms, Curr. Opin. Biotechnol. 17 (4) (2006) 415–421.

[9] C. Situma, M. Hashimoto, S. A. Soper, Merging microfluidics with microarray-based bioassays, Biomol. Eng. 23 (5) (2006) 213–231.

[10] P. Dittrich, A. Manz, Single-molecule fluorescence detection in microflu-

idic channels - the holy grail in μtas?, Anal. Bioanal. Chem. 382 (8) (2005) 1771–1782.

[11] R. E. Kunz, K. Cottier, Optimizing integrated optical chips for label-free (bio-)chemical sensing, Anal. Bioanal. Chem. 384 (1) (2006) 180–190.

[12] I. Caelen, A. Bernard, D. Juncker, B. Michel, H. Heinzelmann, E. Delamarche, Formation of gradients of proteins on surfaces with microfluidic networks, Langmuir 16 (24) (2000) 9125–9130.

[13] B. Goldstein, D. Coombs, X. Y. He, A. R. Pineda, C. Wofsy, The influence of transport on the kinetics of binding to surface receptors: application to cells and biacore, J. Mol. Recognit. 12 (5) (1999) 293–299.

[14] N. T. Nguyen, Z. G. Wu, Micromixers - a review, J. Micromech. Microeng. 15 (2) (2005) R1–R16.

[15] V. Hessel, H. Lowe, F. Schonfeld, Micromixers - a review on passive and active mixing principles, Chem. Eng. Sci. 60 (8-9) (2005) 2479–2501.

[16] M. Abrantes, M. T. Magone, L. F. Boyd, P. Schuck, Adaptation of a surface plasmon resonance biosensor with miorofluidics for use with small sample volumes and long contact times, Anal. Chem. 73 (13) (2001) 2828–2835.

[17] R. A. Vijayendran, K. M. Motsegood, D. J. Beebe, D. E. Leckband, Evaluation of a three-dimensional micromixer in a surface-based biosensor, Langmuir 19 (5) (2003) 1824–1828.

[18] J. P. Golden, T. M. Floyd-Smith, D. R. Mott, F. S. Ligler, Target delivery in a microfluidic immunosensor, Biosens. Bioelectron. 22 (2007) 2763–2767.

[19] A. D. Stroock, S. K. W. Dertinger, A. Ajdari, I. Mezic, H. A. Stone, G. M. Whitesides, Chaotic mixer for microchannels, Science 295 (5555) (2002) 647–651.

[20] H. P. Jennissen, T. Zumbrink, A novel nanolayer biosensor principle, Biosens. Bioelectron. 19 (9) (2004) 987–997.

[21] T. Gervais, K. F. Jensen, Mass transport and surface reactions in microfluidic systems, Chem. Eng. Sci. 61 (2006) 1102–1121.

[22] F. Yu, D. F. Yao, W. Knoll, Surface plasmon field-enhanced fluorescence spectroscopy studies of the interaction between an antibody and its surface-coupled antigen, Anal. Chem. 75 (11) (2003) 2610–2617.

[23] D. G. Myszka, X. He, M. Dembo, T. A. Morton, B. Goldstein, Extending the range of rate constants available from biacore: Interpreting mass transport-influenced binding data, Biophys. J. 75 (2) (1998) 583–594.

[24] T. M. Squires, S. R. Quake, Microfluidics: Fluid physics at the nanoliter scale, Rev. Mod. Phys. 77 (3) (2005) 977–1026.

[25] D. J. Acheson, Elementary Fluid Dynamics, Oxford, Oxford University Press, 1990.

[26] C. Wofsy, B. Goldstein, Effective rate models for receptors distributed in a layer above a surface: Application to cells and biacore, Biophys. J. 82 (4) (2002) 1743–1755.

[27] D. A. Edwards, B. Goldstein, D. S. Cohen, Transport effects on surface-volume biological reactions, J. Math. Biol. 39 (6) (1999) 533–561.

[28] M. K. Liu, P. Li, J. C. Giddings, Rapid protein separation and diffusion-coefficient measurement by frit inlet flow field-flow fractionation, Protein Sci. 2 (9) (1993) 1520–1531.

[29] N. G. Housden, S. Harrison, H. R. Housden, K. A. Thomas, J. A. Beckingham, S. E. Roberts, S. P. Bottomley, M. Graille, E. Stura, M. G. Gore, Observation and characterization of the interaction between a single immunoglobulin binding domain of protein l and two equivalents of human kappa light chains, J. Biol. Chem. 279 (10) (2004) 9370–9378.

[30] L. L. H. Christensen, Theoretical analysis of protein concentration determination using biosensor technology under conditions of partial mass transport limitation, Anal. Biochem. 249 (2) (1997) 153–164.